Physics Letters B 778 (2018) 155–160

Contents lists available at ScienceDirect

Physics Letters B

www.elsevier.com/locate/physletb

Study of spectroscopic factors at $N = 29$ using isobaric analogue resonances in inverse kinematics

J. Bradt [a,b], Y. Ayyad [a,1], D. Bazin [a,b,*], W. Mittig [a,b], T. Ahn [c], S. Beceiro Novo [a,b], B.A. Brown [a,b], L. Carpenter [a,b], M. Cortesi [a], M.P. Kuchera [a,2], W.G. Lynch [a,b], S. Rost [a,b,3], N. Watwood [a,b], J. Yurkon [a], J. Barney [a,b], U. Datta [d], J. Estee [a,b], A. Gillibert [e], J. Manfredi [a,b], P. Morfouace [a,4], D. Pérez-Loureiro [a,5], E. Pollacco [e], J. Sammut [a,b], S. Sweany [a,b]

[a] National Superconducting Cyclotron Laboratory, Michigan State University, East Lansing, MI 48824, USA
[b] Department of Physics and Astronomy, Michigan State University, East Lansing, MI 48824, USA
[c] Department of Physics, University of Notre Dame, Notre Dame, IN 46556, USA
[d] Saha Institute of Nuclear Physics, Kolkata 700 064, India
[e] CEA Irfu, Centre de Saclay, 91191 Gif-sur-Yvette, France

ARTICLE INFO

Article history:
Received 12 October 2017
Received in revised form 20 December 2017
Accepted 8 January 2018
Available online 17 January 2018
Editor: D.F. Geesaman

Keywords:
Spectroscopic factor
Isobaric analogue state
Resonant proton elastic scattering
Shell closure
Single-particle energy

ABSTRACT

Shell closures and their associated magic numbers of nucleons provide a unique means for studying the structure of exotic nuclei far from stability. An experiment was recently performed at the National Superconducting Cyclotron Laboratory to measure resonant elastic proton scattering on ^{46}Ar in inverse kinematics in the region containing isobaric analogue states of ^{47}Ar, an $N = 29$ nucleus with one neutron above the $N = 28$ shell closure. Four candidate resonances were observed: one corresponding to the $3/2^-$ ground state of ^{47}Ar, another corresponding to its $1/2^-$ first excited state, and two that likely correspond to states in the ^{47}K compound nucleus. The observed properties of the ground state resonance were compatible with values from the literature, but a significantly lower spectroscopic factor was found for the $1/2^-$ state resonance.

The study of the evolution of shell closures in nuclei far from stability is an important part of current research in nuclear physics. For example, tensor forces have been found to have a strong influence on the $N = 20$ shell closure in the oxygen isotopes, where a new semi-magic number appears at $N = 16$ [1]. At higher N, nuclei such as ^{48}Ca exhibit the well-established properties of magic numbers at $N = 28$, the lowest magic number in the chart of the nuclides that is caused by spin–orbit splitting. The behavior of shell closures is a privileged benchmark for nuclear structure models because nuclear properties are more easily defined with fewer valence nucleons. In addition to binding energies, the orbitals can be characterized based on their neutron separation energies, deformation, and collectivity [2]. Among the many reaction tools used to study these properties, transfer reactions are widely known to directly provide information on the single-particle properties via the deduction of single-particle energies and spectroscopic factors.

For these reasons, ^{47}Ar ($Z = 18$, $N = 29$) has been the subject of a variety of complementary experiments to study the behavior of the $N = 28$ neutron shell closure two protons below ^{48}Ca. A deduction of the single-particle energies at 10 MeV/u performed at GANIL by Gaudefroy et al. [3,4] led to the conclusion that the spin–orbit splitting between the $p_{3/2}$ and $p_{1/2}$ states is reduced by 45% in ^{47}Ar as compared to the isotone ^{49}Ca. This conclusion was questioned in a comment [5] that described the fragmentation of $p_{1/2}$ strength and noted that one has to take into account the total strength distribution of this single-particle state in order to determine the center of gravity. Gaudefroy et al. [6] addressed this in a reply where they reported a weaker reduction in the spin–orbit splitting.

* Corresponding author at: National Superconducting Cyclotron Laboratory, Michigan State University, East Lansing, MI 48824, USA.
E-mail address: bazin@nscl.msu.edu (D. Bazin).

[1] Present address: Nuclear Science Division, Lawrence Berkeley National Laboratory, Berkeley, CA 94720, USA.
[2] Present address: Department of Physics, Davidson College, Davidson, NC 28035, USA.
[3] Present address: Institute for Advanced Simulation, Forschungszentrum Jülich, 52425 Jülich, Germany.
[4] Present address: GANIL, Boulevard Henri Becquerel, 14000 Caen, France
[5] Present address: Department of Physics and Astronomy, University of Tennessee, Knoxville, TN 37996, USA.

https://doi.org/10.1016/j.physletb.2018.01.015

In a later work by Bhattacharyya et al. [7], states in ^{47}Ar were populated via deep inelastic transfer reactions. They observed many of the states that were seen by the previous measurement, but they also identified several new states, including a new $5/2^-$ state at 1234 keV, only 34 keV above the energy they measured for the $1/2^-$ first excited state.

Most recently, Gade et al. [8] studied ^{47}Ar at the NSCL using one-neutron pickup and one-proton removal reactions measured via γ-ray spectroscopy. This work provided a very precise measurement of all previously known energy levels in the ^{47}Ar nucleus except for the $1/2^-$ first excited state, which could not be populated due to angular momentum coupling constraints.

In this work, we present a study of ^{47}Ar using resonant elastic proton scattering on ^{46}Ar, populating the isobaric analogue states in ^{47}K. To our knowledge, this is the first experiment involving isobaric analogue states in this mass region. It was also the radioactive beam commissioning experiment for the Active-Target Time Projection Chamber (AT-TPC) at the NSCL [9]. During the experiment, 183.5 h of data were recorded, yielding 3×10^4 proton scattering events after data analysis. This letter is focused on the physics results of the experiment; full details about the experimental setup and data analysis procedure are given in Ref. [9].

^{46}Ar was produced from the fragmentation of a 140 MeV/u ^{48}Ca primary beam accelerated by the coupled cyclotrons and selected using the A1900 fragment separator [10]. The ^{46}Ar fragments were then stopped in a linear gas cell and transported to an electron beam ion source (EBIS), where their charge state was increased from 1+ to 17+. Finally, the ions were injected into the ReA3 re-accelerator [11], and accelerated to 4.6 MeV/u. The extraction time of the beam from the EBIS was stretched as much as possible, resulting in non-uniform bunches of length 100 ms every 500 ms, or a duty cycle of 20%. As a result, the instantaneous beam particle rate fluctuated between 5000 Hz and 60 000 Hz, much higher than the average rate of 1180 Hz. Two beam contaminants, ^{46}K (2.2%) and ^{46}Ca (0.4%), were generated through β-decay of ^{46}Ar. An additional heavier contaminant was identified as ^{57}Fe 21+ (27.8%). These were identified using a very thin ion chamber (approximately 500 µg/cm^2 including the isobutane gas at 20 torr and the aluminized plastic windows) located upstream of the AT-TPC [9].

The beam entered the active volume of the AT-TPC through a 3.6 µm thick aluminized para-aramid (aromatic polyamide fibers also known as Kevlar) window of 1 cm diameter. The AT-TPC active volume is a cylinder of length 1 m and radius 29.2 cm, which was filled with isobutane (C_4H_{10}) at 19.2 torr and placed in a uniform 1.68 T magnetic field generated by a solenoidal magnet. At this pressure, the beam particles were stopped several centimeters before the sensor plane mounted on the downstream end of the active volume. The sensor plane consists of a mosaic of 10 240 equilateral triangles (or *pads*) that provide the x and y information for the tracks, while the signal from each pad is sampled into a 512-sample switched capacitor array at a frequency of 12.5 MHz. The timing information from the signals is then used to deduce the z component of the tracks, or the component along the drift direction in the detector. From the measured electron drift velocity of 5.2 cm/µs, each sample corresponds to 4.2 mm in the drift direction.

The amplification, sampling and readout of the detector was performed by a dedicated electronics system [12] triggered by the presence of track signals outside the pad region illuminated by the beam particles. The timing of the trigger was established from the ion chamber signal in order to retain the arrival of beam particles through the window as time reference, essential to the determination of the reaction vertex position along the beam axis. The average trigger rate was approximately 10 Hz. Complete details about the electronics and trigger setup can be found in [9,13].

The observation of isobaric analogue resonances using resonant proton scattering was first reported on ^{88}Sr and ^{89}Y [14,15]. This type of reaction was quickly recognized as a valid tool to extract spectroscopic factors [16], and its relation to the determination from transfer reactions such as (d,p) established [17]. The observation of isobaric analogue states of ^{41}Ar in ^{41}K was similarly done through resonances observed in the elastic scattering of protons on ^{40}Ar by Scott et al. [18]. They noted that the elastic scattering width Γ_p is related to the spectroscopic factor of a state of spin-parity J^π by the relation

$$S_{J^\pi} = \frac{(2T_0 + 1)\Gamma_p}{\Gamma_{\mathrm{sp}}}, \tag{1}$$

where $2T_0 + 1 = N - Z$ for the parent nucleus, and Γ_{sp} is the single-particle width as determined either by the R matrix model or by the resonance width for proton scattering in an optical model potential. Similarly to Scott et al. [18], the present experiment was designed to observe resonances in the excitation function. The resonance for an isobaric analogue state is expected in the center-of-mass frame at

$$E_{\mathrm{res}} = E_x(A + 1, Z) + \Delta E_C - S_n(A + 1, Z). \tag{2}$$

Here, $E_x(A + 1, Z)$ is the excitation energy in the ^{47}Ar nucleus, ΔE_C is the Coulomb displacement energy (which can be calculated from an empirical formula [19,20]), and $S_n(A + 1, Z)$ is the neutron separation energy. Using values of $\Delta E_C = 6.282$ MeV and $S_n = 3.665(2)$ MeV [21] yields a resonance energy of $E_{\mathrm{res}} = 2.617$ MeV for the ground state. For comparison, the energy of the re-accelerated ^{46}Ar after the ion chamber and the AT-TPC entrance window was 4.17 MeV/u. This allows the measurement of resonances corresponding to excitation energies up to 1.5 MeV. This energy domain contains the $3/2^-$ ground state, a $1/2^-$ state at 1130 keV [4], and a $5/2^-$ state at 1231 keV [8]. Note that the excitation energies of these resonances in the ^{47}K compound nucleus are much higher than in the ^{40}Ar case measured by Scott et al. [18], so the level densities are much higher, and the fine-structure resonance components are therefore not observable within our experimental resolution.

A typical proton track recorded by the AT-TPC is shown in Fig. 1. The tracks were analyzed using a multi-step process which is described in detail in Ref. [9]. First, the tracks were identified and separated from noise using a process [22–25] based on the Hough transform [26]. This removed spurious points in the 3D track reconstruction that arise from cross-talk in the electronics and from random triggers due to the low discriminator threshold applied to each channel. The Hough transform results were used as a starting point for a Monte Carlo minimization in the 6-dimensional space given by the reaction vertex location (x_0, y_0, z_0), the reaction vertex energy E_0, and the two angles (θ_0, ϕ_0) describing the orientation of the proton's momentum vector at the reaction vertex. The Monte Carlo algorithm minimizes the difference between a simulated track and the experimental hit pattern. The track simulation accounts for the staggered division of charge deposited on adjacent triangular pads, the energy-dependent energy loss as given by SRIM [27], and the lateral diffusion of the drift electrons. An example of the fit results is shown in Fig. 1. At this stage, scattering on carbon nuclei from the C_4H_{10} molecules could be eliminated because the energy loss of the recoiling carbon nucleus is very different from that of the protons.

One important quality factor for the present data is the energy resolution of the excitation function. This resolution was obtained by fitting the high-energy edge of the ^{46}Ar vertex energy spectrum with a modified Gaussian cumulative distribution function as

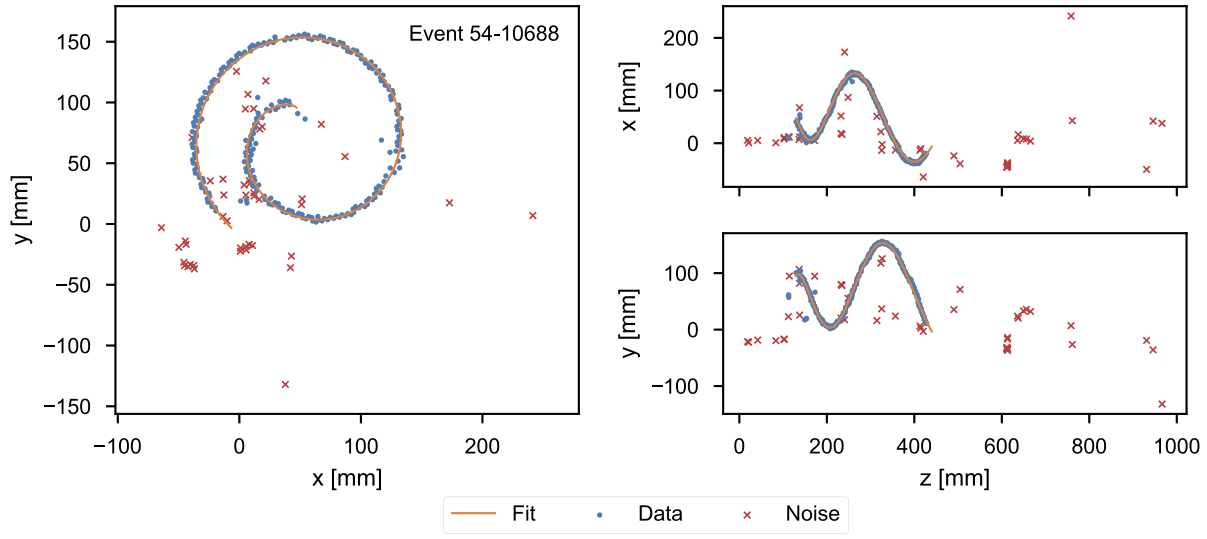

Fig. 1. A typical proton recoil spiral as observed in the AT-TPC in the reaction ^{46}Ar(p, p). The points labeled "data" were identified as part of the track, while the points labeled "noise" were rejected as noise. The Monte Carlo fit is also shown, including an extrapolation from the first data point back to the beam axis to find the vertex position. This proton had an energy of 1.57 MeV/u and a scattering angle of 62.3° in the laboratory frame.

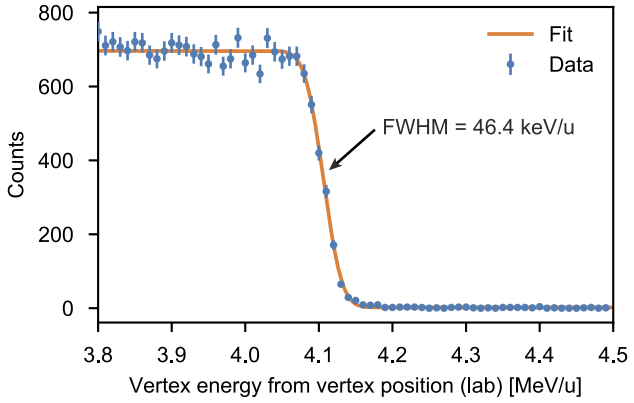

Fig. 2. The number of events as a function of the ^{46}Ar nucleus energy at the reaction vertex. The sharp cutoff at 4.11 MeV/u corresponds to the entrance window of the AT-TPC.

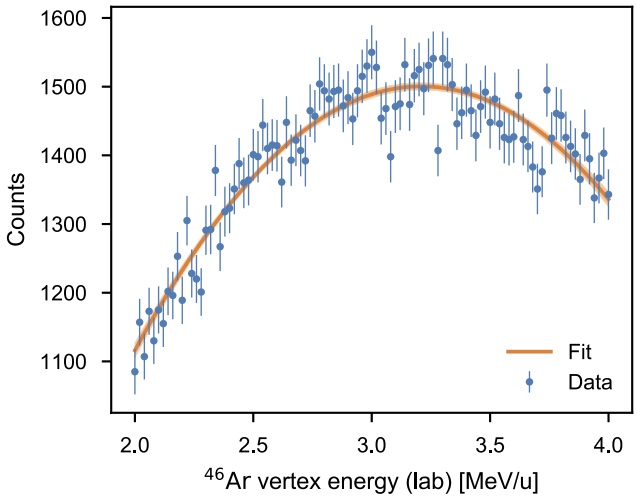

Fig. 3. Experimental counts, summed over all scattering angles. A quadratic fit is shown with a 1σ error band.

shown in Fig. 2, yielding a FWHM resolution of 46 keV/u. This result is within the resolution needed for the present experiment. The energy straggling of the beam in the entrance window, the ion chamber, and the gas was calculated with SRIM [27] down to an energy of approximately 2 MeV/u and was found to be less than 10 keV/u. The scattering angle and energy acceptances of the AT-TPC in the present experiment were limited by the trigger generation, especially at forward scattering angles in the laboratory frame, where the track multiplicity is low due to the small projection of each track onto the sensor plane. Due to these trigger limitations, the angular domain of the data was restricted to the region between roughly 30° and 65° in the center-of-mass frame. Resonance effects are smaller in this angular domain than at very backwards angles in the center-of-mass frame; however, this is compensated for by much higher cross sections. The non-resonant scattering is predominantly Rutherford scattering, limiting the influence of optical model parameter uncertainties.

The counts were summed over all scattering angles to produce the data shown in Fig. 3. Theoretically, this data consists of resonances superimposed on a slowly varying baseline. This baseline was modeled using a quadratic function and then removed using the formula

$$S(E) = \frac{N(E) - B(E)}{B(E)} \tag{3}$$

where $N(E)$ represents the data, $B(E)$ is the baseline, and $S(E)$ is the resulting baseline-subtracted normalized data. This baseline-subtracted normalized data was then fit using an R matrix model to estimate the properties of the observed resonances. The R matrix calculation was performed using the DSigmaIV program [28,29], which is based on the Lane and Thomas [30] description of the theory. The Koning and Delaroche [31] global optical potential was used for the elastic scattering component of the reaction. After performing the calculation, the results were summed over all scattering angles with weights that were proportional to the number of experimental counts observed in each angular bin. The non-resonant elastic scattering component was then removed from this weighted sum by comparing the results to an R matrix calculation without resonances and finding the normalized difference in the same way as was done for the data. Finally, this renormalized, summed R matrix curve was convoluted with a Gaussian with full width at half maximum of 46 keV/u to model the energy resolution of the detector.

Table 1
Properties of the resonances shown in Fig. 4. Energies and widths are given in keV/u. $E_{\mathrm{res}}^{\mathrm{CM}}$ is the resonance energy in the center of mass frame; E_x is the excitation energy calculated from the resonance assuming $\Delta E_C - S_n = 2680(20)$ keV, the energy of the ground state resonance; J^π gives the spin and parity assigned to the resonance; T_z indicates the isospin projection; S refers to the spectroscopic factor; Γ is the total resonance width; and Γ_p is the proton width. For quantities with two uncertainties, the first value is the systematic uncertainty and the second is statistical.

$E_{\mathrm{res}}^{\mathrm{CM}}$ (keV)	E_x (keV)	J^π	T_z	S	Γ (keV)	Γ_p (keV)	F	p
$2680 \pm 108 \pm 20$	$0 \pm 91 \pm 28$	$3/2^-$	11/2 (^{47}Ar)	$0.27 \pm 0.03\ ^{+0.21}_{-0.13}$	15(10)	4.3(4)	2.14	0.15
$2990\ ^{+117}_{-124} \pm 20$	$310\ ^{+91}_{-92} \pm 28$	$1/2^+$	9/2 (^{47}K)	$0.027 \pm 0.006\ ^{+0.013}_{-0.007}$	30(10)	20(2)	3.59	0.04
$3280\ ^{+125}_{-127} \pm 20$	$600\ ^{+92}_{-93} \pm 28$	$1/2^+$	9/2 (^{47}K)	$0.008 \pm 0.002\ ^{+0.005}_{-0.006}$	18(10)	8.0(8)	0.68	0.58
$3650\ ^{+137}_{-147} \pm 20$	$970\ ^{+95}_{-99} \pm 28$	$1/2^-$	11/2 (^{47}Ar)	$0.42 \pm 0.05 \pm 0.09$	34(10)	24(2)	5.50	0.01

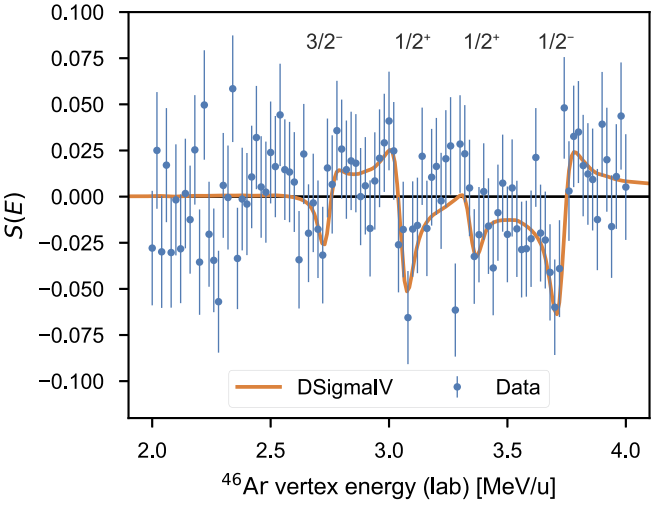

Fig. 4. Comparison between data and R matrix calculation.

The experimental data is compared to the R matrix calculation in Fig. 4, where four candidate resonances are seen. The resonance parameters were optimized by manually adjusting the resonance energies and spectroscopic factors used as input to DSigmaIV. The resonance widths were calculated by this code as a function of those parameters. A resonance mixing phase of 20° was included to account for averaging over the fine structure components of the resonances [32,18], and a resonance spreading width of 10 keV was included to account for splitting over these states [33,32]. The resulting resonance properties are shown in Table 1.

The systematic uncertainty of the resonance energy $E_{\mathrm{res}}^{\mathrm{CM}}$ includes a component from the calibration process, a component that accounts for an estimated 5% uncertainty in the drift velocity, and a component from the uncertainty in the relative Coulomb shifts between levels. This last uncertainty was taken to be 64 keV from the systematic comparison review on light nuclei done in [34]. The systematic uncertainty of the excitation energy E_x is smaller because the calibration and drift velocity uncertainties are highly correlated between states, leading to a large covariance. The systematic uncertainty of the spectroscopic factors was estimated from the uncertainty in the height of the resonance peaks.

An F test was performed around each resonance to establish the level of statistical significance of the experimental results. This test compared the R matrix model shown in Fig. 4 to a null model that consists of a horizontal line passing through the origin. The comparison was made using the F statistic

$$F = \frac{(\mathrm{RSS}_0 - \mathrm{RSS}_R)/(\nu_0 - \nu_R)}{\mathrm{RSS}_R/\nu_R}, \tag{4}$$

where RSS is the residual sum of squares, ν is the number of degrees of freedom, and subscripts R and 0 refer to the R matrix model and the null model, respectively. The value of this statistic was calculated for each peak and compared to an F distribution to find a p-value for each peak that corresponds to the probability of observing a more-extreme deviation from the baseline assuming the null model is true. If this p-value was less than a predetermined threshold of 0.10, then the null model was rejected in favor of the R matrix model, and the resonance was deemed statistically significant. The calculated p-values and the values of the F statistic are shown in Table 1. At the 10% level, the lower-energy $1/2^+$ resonance and the $1/2^-$ resonance were statistically significant. The p-value calculated for the entire energy range (including all four resonances) was < 0.01 ($F = 2.81$).

Two of the four resonances listed in Table 1 correspond to isobaric analogues of states in ^{47}Ar. The 2680 keV resonance was identified as the analogue of the ground state of ^{47}Ar, and the 3650 keV resonance corresponds to its $1/2^-$ first excited state. The remaining two $1/2^+$ resonances do not correspond to known states in ^{47}Ar, so they were identified as resonances with a lower isospin projection which arise from unbound states in the ^{47}K compound nucleus. The spectroscopic factors of these resonances were therefore calculated without the factor of $2T_0 + 1 = 11$ from Eq. (1).

The values deduced in the present experiment are compared to several previous determinations and shell model calculations in Fig. 5. Our determination of the properties of the ground state are compatible with the previous experiment within 2σ, but the observed parameters of the first excited $1/2^-$ state do not agree with the literature values. The observed excitation energy of this state is somewhat lower than the previously reported value of 1130 keV [4]. This is compatible with the previously mentioned fluctuations in the Coulomb shift and the experimental error.

Several factors may influence the absolute spectroscopic factor as deduced from the R matrix analysis of the present work.

- Optical model parameters used: in the angular and energy domain of the present work the potential scattering amplitude is dominated by Rutherford so the main influence will come from the phases in the resonant term that interferes with the potential scattering.
- Spreading width: a resonance integral, defined as the integral of the deviation from unity in Fig. 4, was used to quantify the resonance effect. It was checked that this quantity was not very sensitive to variations of the spreading width, less than 10%.
- Resonance mixing phase: the resonance mixing phase changes the interference pattern between the potential and resonant amplitudes. Introducing the value of 20° from [32,18] improved the fit for the $1/2^-$ resonance for example. From our rough estimation, a reasonable variation of the resonance

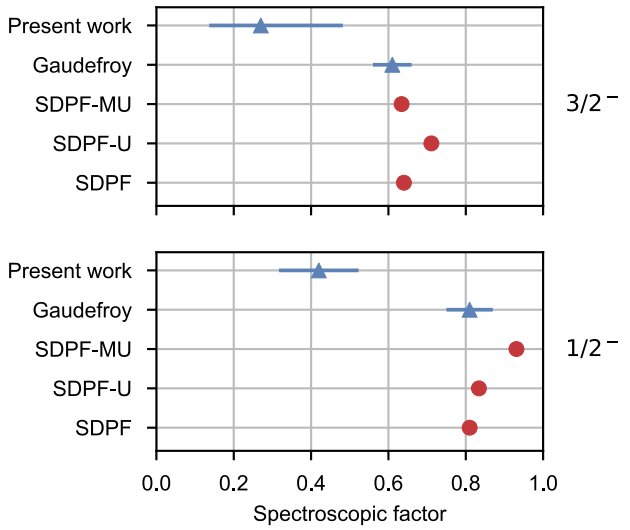

Fig. 5. Comparison of deduced spectroscopic factors to literature values. Blue triangles represent experimentally deduced results, while red circles represent shell model calculations. The error bars for the present work include both statistical and systematic errors. The shell-model calculations are taken from [3] for SDPF and [8] for SDPF-M and SDPF-MU. (For interpretation of the references to color in this figure legend, the reader is referred to the web version of this article.)

phase should not change the spectroscopic factor by more than 20%.

- Single particle width: The single particle resonance width was calculated in a real optical model potential. The values obtained with the optical model were 30±10% smaller than the R-matrix, therefore giving a 30% bigger spectroscopic factor than the R-matrix value. One would not expect an error bigger than 20% for the single particle reference, a value also typical for (d,p) analysis.

All these factors should not add up to more that 30% uncertainty, except if there are unexpected large deviations from the ingredients used. Note that (d,p) measurements have rarely a precision better than 20–30%.

One potential explanation for the lower spectroscopic factor we deduce for the $1/2^-$ state could be the presence of a nearby $5/2^-$ state that was first observed by Bhattacharyya et al. [7] only 34(7) keV above the $1/2^-$ state. Within the 75 keV experimental resolution of Gaudefroy et al. [4], it would not have been possible to separate this state from the $1/2^-$ state. Although this hypothesis is not supported by the shape of the angular distribution observed for the $1/2^-$ state in the (d,p) reaction, the spectroscopic factor reported by Gaudefroy et al. [4] for the $1/2^-$ state may be larger than the actual value if it includes a significant contribution from transfer into the $5/2^-$ state. This $5/2^-$ state does not have a significant effect on the spectroscopic factor deduced in the present experiment, however, since the probability of populating it in a (p, p) reaction is negligible compared to the probability in a (d, p) reaction due to the low penetrability of this partial wave.

A smaller spectroscopic factor for the $1/2^-$ state could imply a shift in the $2p_{1/2}$ single-particle energy and the spin–orbit splitting of the $2p$ orbitals in the ^{47}Ar nucleus. Single-particle energies are calculated as the weighted sum of the experimental energy levels having the same spin and parity as the single-particle state, where the weights are given by the spectroscopic factors. Thus, if the spectroscopic factor of this lowest-lying $1/2^-$ state is smaller than was previously reported, the single-particle energy of the $2p_{1/2}$ orbital will be larger since the higher-energy $1/2^-$ states must contribute more significantly to the sum. Assuming the $2p_{3/2}$ single-particle energy remains unchanged, this would imply a larger spin–orbit splitting between the two $2p$ orbitals. These changes in splitting could be explained by larger-than-expected nuclear deformation in ^{47}Ar. These possibilities rely on the single observation of a smaller spectroscopic factor for the analog resonance of the $1/2^-$ state in ^{47}Ar, and are in contradiction with most shell model calculations as shown in Fig. 5. Clearly, more precise measurements that reconciles the ground state spectroscopic factor and the value deduced in the (d,p) reaction are needed before a firm conclusion can be drawn.

We finally discuss the shell-model configurations related to the observed $1/2^+$ resonances. Note that the second $1/2^+$ resonance is not significant by the statistical analysis criteria shown in Table 1. The excitation energies of these resonances in ^{47}K are at 15.988 MeV and 16.278 MeV, respectively. The neutron decay Q-value of 7–8 MeV implies a large single-particle neutron decay width of the order of 5 MeV. The upper limit on the neutron decay widths of about 10 keV therefore implies neutron decay spectroscopic factors smaller than about 0.002. The spectroscopic factor deduced from the observed proton width of the first $1/2^+$ resonance is larger by an order of magnitude. The neutron decay is allowed only via the admixture of small components of the $1/2^+$ ground state of ^{47}K to the complex 2p–2h states. On the other hand, the proton decay may originate from the fragmented 2s proton single particle state in this energy region.

In summary, we have observed in the commissioning experiment of the AT-TPC isobaric analogue states of ^{47}Ar in the excitation function of the elastic scattering reaction ^{46}Ar(p, p) in inverse kinematics. The specific properties of active target technology allowed us to measure the excitation function over a broad energy range with a center-of-mass energy resolution of 46 keV at a mean beam intensity of 1200 Hz. This allowed us to extract the spectroscopic factors for the $3/2^-$ ground state and the $1/2^-$ first excited state of ^{47}Ar and compare the values to results obtained from a (d, p) reaction. We anticipate a better scattering angle acceptance in future experiments through the use of a true global multiplicity trigger module. Additionally, the statistics of future proton scattering experiments will be enhanced by the larger density of proton scattering centers provided by pure hydrogen gas, which can now be used in the AT-TPC thanks to the additional electron amplification provided by a new thick GEM (Gas Electron Multiplier) device installed in front of the Micromegas [35]. Finally, a special set of front-end electronics has been developed to polarize individual pads independently in order to reduce the electron gain by several orders of magnitude on these pads only; this will help reduce the recurrence of the noise and saturation effects seen in this experiment since those were mainly caused by the large number of avalanche electrons incident on the pads from the ^{46}Ar beam particle tracks [9]. This pioneering experiment and further technical improvements open the possibility of using isobaric analogue states to study the structure of medium- and heavy-mass nuclei far from stability with intensities on the order of 1 kHz.

Acknowledgements

The authors are indebted to A. Gade for fruitful guidance and discussions. This experiment was supported by the National Science Foundation (NSF) under cooperative agreement no. PHY-1102511 and grant no. PHY-1404442. Construction of the AT-TPC was partially supported by the NSF under grant no. MRI-0923087. Computational resources were provided by the Institute for Cyber-Enabled Research at Michigan State University.

References

[1] T. Otsuka, T. Suzuki, R. Fujimoto, H. Grawe, Y. Akaishi, Evolution of nuclear shells due to the tensor force, Phys. Rev. Lett. 95 (2005) 232502, https://doi.org/10.1103/PhysRevLett.95.232502.

[2] O. Sorlin, M.-G. Porquet, Evolution of the N = 28 shell closure: a test bench for nuclear forces, Phys. Scr. T 152 (2013) 014003, https://doi.org/10.1088/0031-8949/2013/T152/014003.

[3] L. Gaudefroy, O. Sorlin, D. Beaumel, Y. Blumenfeld, Z. Dombrádi, S. Fortier, S. Franchoo, M. Gélin, J. Gibelin, S. Grévy, F. Hammaehe, F. Ibrahim, K. Kemper, K.L. Kratz, S.M. Lukyanov, C. Monrozeau, L. Nalpas, F. Nowacki, A.N. Ostrowski, Y.E. Penionzhkevich, E. Pollacco, P. Roussel-Chomaz, E. Rieh, J.A. Scarpaci, M.G. St Laurent, T. Rauscher, D. Sohler, M. Stanoiu, E. Tryggestad, D. Verney, Study of the N = 28 shell closure in the Ar isotopic chain: a SPIRAL experiment for nuclear astrophysics, Eur. Phys. J. A 27 (Suppl. 1) (2006) 309–314, https://doi.org/10.1140/epja/i2006-08-047-0.

[4] L. Gaudefroy, O. Sorlin, D. Beaumel, Y. Blumenfeld, Z. Dombrádi, S. Fortier, S. Franchoo, M. Gélin, J. Gibelin, S. Grévy, F. Hammache, F. Ibrahim, K.W. Kemper, K.L. Kratz, S.M. Lukyanov, C. Monrozeau, L. Nalpas, F. Nowacki, A.N. Ostrowski, T. Otsuka, Y.E. Penionzhkevich, J. Piekarewicz, E.C. Pollacco, P. Roussel-Chomaz, E. Rich, J.A. Scarpaci, M.G. St. Laurent, D. Sohler, M. Stanoiu, T. Suzuki, E. Tryggestad, Reduction of the spin–orbit splittings at the N=28 shell closure, Phys. Rev. Lett. 97 (9) (2006) 092501, https://doi.org/10.1103/PhysRevLett.97.092501.

[5] A. Signoracci, B.A. Brown, Comment on "Reduction of the spin–orbit splittings at the N=28 shell closure", Phys. Rev. Lett. 99 (9) (2007) 099201, https://doi.org/10.1103/PhysRevLett.99.099201.

[6] L. Gaudefroy, O. Sorlin, D. Beaumel, Y. Blumenfeld, Z. Dombrádi, S. Fortier, S. Franchoo, M. Gélin, J. Gibelin, S. Grévy, F. Hammache, F. Ibrahim, K.W. Kemper, K.L. Kratz, S.M. Lukyanov, C. Monrozeau, L. Nalpas, F. Nowacki, A.N. Ostrowski, T. Otsuka, Y.E. Penionzhkevich, J. Piekarewicz, E.C. Pollacco, P. Roussel-Chomaz, E. Rich, J.A. Scarpaci, M.G. St. Laurent, D. Sohler, M. Stanoiu, T. Suzuki, E. Tryggestad, D. Verney, Reply, Phys. Rev. Lett. 99 (9) (2007) 099202, https://doi.org/10.1103/PhysRevLett.99.099202.

[7] S. Bhattacharyya, M. Rejmund, A. Navin, E. Caurier, F. Nowacki, A. Poves, R. Chapman, D. O'Donnell, M. Gelin, A. Hodsdon, X. Liang, W. Mittig, G. Mukherjee, F. Rejmund, M. Rousseau, P. Roussel-Chomaz, K.M. Spohr, C. Theisen, Structure of neutron-rich Ar isotopes beyond N=28, Phys. Rev. Lett. 101 (3) (2008) 032501, https://doi.org/10.1103/PhysRevLett.101.032501.

[8] A. Gade, J.A. Tostevin, V. Bader, T. Baugher, D. Bazin, J.S. Berryman, B.A. Brown, C.A. Diget, T. Glasmacher, D.J. Hartley, E. Lunderberg, S.R. Stroberg, F. Recchia, A. Ratkiewicz, D. Weisshaar, K. Wimmer, Single-particle structure at N=29: the structure of ^{47}Ar and first spectroscopy of ^{45}S, Phys. Rev. C 93 (5) (2016) 054315, https://doi.org/10.1103/PhysRevC.93.054315.

[9] J. Bradt, D. Bazin, F. Abu-Nimeh, T. Ahn, Y. Ayyad, S. Beceiro Novo, L. Carpenter, M. Cortesi, M. Kuchera, W. Lynch, W. Mittig, S. Rost, N. Watwood, J. Yurkon, Commissioning of the active-target time projection chamber, Nucl. Instrum. Methods Phys. Res., Sect. A, Accel. Spectrom. Detect. Assoc. Equip. 875 (2017) 65–79, https://doi.org/10.1016/j.nima.2017.09.013.

[10] D.J. Morrissey, B.M. Sherrill, M. Steiner, A. Stolz, I. Wiedenhoever, Commissioning the A1900 projectile fragment separator, Nucl. Instrum. Methods B 204 (2003) 90–96, https://doi.org/10.1016/S0168-583X(02)01895-5.

[11] A.C.C. Villari, D. Alt, G. Bollen, D.B. Crisp, M. Ikegami, S.W. Krause, A. Lapierre, S.M. Lidia, D.J. Morrissey, S. Nash, R.J. Rencsok, R. Ringle, S. Schwarz, R. Shane, C. Sumithrarachchi, S.J. Williams, Q. Zhao, Commissioning and First Accelerated Beams in the Reaccelerator (ReA3) of the National Superconducting Cyclotron Laboratory, MSU, in: Proceedings of IPAC2016, Busan, South Korea, 2016, pp. 4–7.

[12] E. Pollacco, S. Anvar, H. Baba, P. Baron, D. Bazin, C. Belkhiria, B. Blank, J. Chavas, P. Chomaz, E. Delagnes, F. Druillole, P. Hellmuth, C. Huss, E. Galyaev, B. Lynch, W. Mittig, T. Murakami, L. Nalpas, J.-L. Pedroza, R. Raabe, J. Pibernat, B. Raine, A. Rebii, A. Taketani, F. Saillant, D. Suzuki, N. Usher, G. Wittwer, GET: a generic electronic system for TPCs for nuclear physics experiments, Phys. Proc. 37 (2012) 1799–1804, https://doi.org/10.1016/j.phpro.2012.02.506.

[13] J. Bradt, Measurement of Isobaric Analogue Resonances of ^{47}Ar with the Active-Target Time Projection Chamber, Ph.D., Michigan State University, 2017.

[14] J.D. Fox, C.F. Moore, D. Robson, Excitation of isobaric analog states in ^{89}Y and ^{90}Zr, Phys. Rev. Lett. 12 (1964) 198–200, https://doi.org/10.1103/PhysRevLett.12.198, https://link.aps.org/doi/10.1103/PhysRevLett.12.198.

[15] L. Lee, A. Marinov, J. Schiffer, Isobaric-analogue states in Cu65, Phys. Lett. (ISSN 0031-9163) 8 (5) (1964) 352–354, https://doi.org/10.1016/S0031-9163(64)80030-5, http://www.sciencedirect.com/science/article/pii/S0031916364800305.

[16] D. Robson, Theory of isobaric-spin analogue resonances, Phys. Rev. 137 (1965) B535–B546, https://doi.org/10.1103/PhysRev.137.B535, https://link.aps.org/doi/10.1103/PhysRev.137.B535.

[17] C.F. Moore, P. Richard, C.E. Watson, D. Robson, J.D. Fox, Isobaric analogue states in heavy nuclei. I. Molybdenum isotopes, Phys. Rev. 141 (1966) 1166–1179, https://doi.org/10.1103/PhysRev.141.1166, https://link.aps.org/doi/10.1103/PhysRev.141.1166.

[18] H.L. Scott, W. Galati, J.L. Weil, M.T. McEllistrem, Proton-induced reactions on ^{40}Ar and analogs of ^{41}Ar levels, Phys. Rev. 172 (4) (1968) 1139–1148, https://doi.org/10.1103/PhysRev.172.1139.

[19] J. Kantele, Handbook of Nuclear Spectrometry, Academic Press, London, 1995.

[20] M.S. Antony, J. Britz, A. Pape, Coulomb displacement energies between analog levels for $44 \leq A \leq 239$, At. Data Nucl. Data Tables 40 (1) (1988) 9–56, https://doi.org/10.1016/0092-640X(88)90003-4.

[21] National Nuclear Data Center, Q-value calculator, https://www.nndc.bnl.gov/qcalc/index.jsp, 2017, based on M. Wang et al., Chin. Phys. C 41 (2017) 03003.

[22] Y. Ayyad, W. Mittig, D. Bazin, M. Cortesi, Overview of the data analysis and new micro-pattern gas detector development for the Active Target Time Projection Chamber (AT-TPC) project, J. Phys. Conf. Ser. 876 (1) (2017) 012003, https://doi.org/10.1088/1742-6596/876/1/012003.

[23] Y. Ayyad, Analysis methods for the AT-TPC, Nucl. Instrum. Methods Phys. Res., Sect. A, Accel. Spectrom. Detect. Assoc. Equip., forthcoming.

[24] J. Illingworth, J. Kittler, The adaptive Hough transform, IEEE Trans. Pattern Anal. Mach. Intell. PAMI-9 (5) (1987) 690–698, https://doi.org/10.1109/TPAMI.1987.4767964.

[25] I. Heinze, Development of a Hough Transformation Track Finder for Time Projection Chambers, Ph.D., University of Hamburg, 2013.

[26] R.O. Duda, P.E. Hart, Use of the Hough transformation to detect lines and curves in pictures, Commun. ACM 15 (1) (1972), https://doi.org/10.1145/361237.361242.

[27] J.F. Ziegler, M.D. Ziegler, J.P. Biersack, SRIM – The stopping and range of ions in matter (2010), Nucl. Instrum. Methods B 268 (11–12) (2010) 1818–1823, https://doi.org/10.1016/j.nimb.2010.02.091.

[28] H.-W. Wang, L.-M. Duan, X.-H. Yuan, F. Fu, Study of unbound nuclei ^{11}N resonance energy level, High Energy Phys. Nucl. Phys. 30 (1) (2006) 1–4.

[29] H.-W. Wang, Y.-G. Ma, X.-Z. Cai, W.-D. Tian, D.-Q. Fang, J.-G. Chen, W. Guo, K. Wang, G.-C. Lu, C.-W. Ma, G.-H. Liu, Y. Shi, E.-J. Ma, Q.-M. Su, T.-Z. Yan, Structure study of light unbound nuclei near drip line, Chin. Phys. C 32 (Suppl. II) (2008) 38–40.

[30] A.M. Lane, R.G. Thomas, R-matrix theory of nuclear reactions, Rev. Mod. Phys. 30 (2) (1958) 257, https://doi.org/10.1103/RevModPhys.30.257.

[31] A.J. Koning, J.P. Delaroche, Local and global nucleon optical models from 1 keV to 200 MeV, Nucl. Phys. A 713 (3–4) (2003) 231–310, https://doi.org/10.1016/S0375-9474(02)01321-0.

[32] H.L. Harney, Determination of spectroscopic factors from elastic proton scattering through the isobaric analogue resonances, Nucl. Phys. A 119 (3) (1968) 591–608, https://doi.org/10.1016/0375-9474(68)90261-3.

[33] J. Reiter, H.L. Harney, Isospin mixing matrix elements extracted from isobaric analog resonances, Z. Phys. A 337 (2) (1990) 121–129, https://doi.org/10.1007/BF01294282.

[34] R.D. Meijer, H.V. Royen, P. Brussaard, Calculation of Coulomb displacement energies in light nuclei, Nucl. Phys. A (ISSN 0375-9474) 164 (1) (1971) 11–33, https://doi.org/10.1016/0375-9474(71)90840-2, http://www.sciencedirect.com/science/article/pii/0375947471908402.

[35] M. Cortesi, S. Rost, W. Mittig, Y. Ayyad-Limonge, D. Bazin, J. Yurkon, A. Stolz, Multi-layer thick gas electron multiplier (M-THGEM): a new MPGD structure for high-gain operation at low-pressure, Rev. Sci. Instrum. 88 (1) (2017) 013303, https://doi.org/10.1063/1.4974333.